L-Band Radiometric Measurement of Liquid Water in Greenland's Firn: Comparative Analysis with In Situ Measurements and Modeling

Journal:	*Annals of Glaciology*
Manuscript ID	Draft
Manuscript Type:	Article
Date Submitted by the Author:	n/a
Complete List of Authors:	Moon, Taylor; University of Montana, Geoscience Harper, Joel; Department of Geosciences, University of Montana, Geosciences Colliander, Andreas ; Jet Propulsion Laboratory Hossan, Alamgir; Jet Propulsion Laboratory Humphrey, Neil; University of Wyoming, Geol
Keywords:	Polar firn, Remote sensing, Ice-sheet modelling, Glacier hydrology
Abstract:	The addition and refreezing of liquid water to Greenland's accumulation area are increasingly important processes for assessing the ice sheet’s present and future mass balance, but uncertain initial conditions, complex infiltration physics, and limited field data pose challenges. Satellite-based L-band radiometry offers a promising new tool for observing liquid water in the firn layer, although further validation is needed. This paper compares time series of liquid water amount (LWA) from three percolation zone sites generated by two model-based and two observation-based methods. LWA is a useful metric for quantifying firn evolution, offering insights into meltwater processes and model performance. LWA integrates the interplay of liquid water generation and refreezing, which often occur simultaneously and repeatedly within firn layers on diurnal, episodic, and seasonal scales. The four LWA records showed average discrepancies of up to 62% nRMSE, reflecting shortcomings inherent to each method. Better agreement between series occurred after excluding the regional climate model record, lowering nRMSE to 8%-13%. The agreement between L-band radiometry and other LWA records inspires confidence in this observational tool for advancing understanding of firn meltwater processes and serving as a

	validation target for simulations of water generation, infiltration, and refreezing in Greenland's melting firn layer.

L-Band Radiometric Measurement of Liquid Water in Greenland's Firn: Comparative Analysis with In Situ Measurements and Modeling

Taylor Moon[1], Joel Harper[1], Andreas Colliander[2], Alamgir Hossan[2], Neil Humphrey[3]

[1]Geosciences, Univ. of Montana
[2]NASA Jet Propulsion Laboratory, California Institute of Technology
[3]Geology/Geophysics, Univ. of Wyoming

Abstract

The addition and refreezing of liquid water to Greenland's accumulation area are increasingly important processes for assessing the ice sheet's present and future mass balance, but uncertain initial conditions, complex infiltration physics, and limited field data pose challenges. Satellite-based L-band radiometry offers a promising new tool for observing liquid water in the firn layer, although further validation is needed. This paper compares time series of liquid water amount (LWA) from three percolation zone sites generated by two model-based and two observation-based methods. LWA is a useful metric for quantifying firn evolution, offering insights into meltwater processes and model performance. LWA integrates the interplay of liquid water generation and refreezing, which often occur simultaneously and repeatedly within firn layers on diurnal, episodic, and seasonal scales. The four LWA records showed average discrepancies of up to 62% nRMSE, reflecting shortcomings inherent to each method. Better agreement between series occurred after excluding the regional climate model record, lowering nRMSE to 8%-13%. The agreement between L-band radiometry and other LWA records inspires confidence in this observational tool for advancing understanding of firn meltwater processes and serving as a validation target for simulations of water generation, infiltration, and refreezing in Greenland's melting firn layer.

1. Introduction

The percolation zone of the Greenland Ice Sheet is the lower-elevation portion of the accumulation zone, experiencing relatively strong surface melting during the summer months (Benson, 1962). At higher and colder elevations of the percolation zone, the meltwater infiltrates to variable depths within the thick package of underlying firn (Amory et al., 2024). This infiltration occurs through two modes of unsaturated flow, the downward propagation of a wetting front and via flow along preferential paths ("piping" events) (Marsh & Woo, 1984). Estimates are that 40% to as much as 70% of the meltwater generated on the surface is retained in the firn layer (e.g., Reijmer et al., 2012; Steger et al., 2017; Vandecrux et al., 2020). Understanding retention processes and time-changes therein within Greenland's firn layer is crucial for both current and future ice sheet mass balance assessments and projections of sea level rise.

To effectively model percolation zone processes, it is essential to first estimate the meltwater generated from the surface energy balance, then accurately simulate the infiltration processes, and finally account for the energies associated refreezing phase change. However, the inherent uncertainties in the initial conditions and the complexities of the underlying physics pose significant modeling challenges. The difficulties of acquiring field data from the percolation zone results in few observational datasets for developing and validating firn models in wet conditions. An emerging observational tool is satellite-based L-band radiometry, providing information on the volume of liquid water retained in the firn layer at any given time (e.g., Houtz et al., 2021; Mousavi et al., 2021; Colliander et al., 2022; Hossan et al., 2024).

At times when melt generation in the percolation zone is sufficiently robust and sustained, a surface wet layer forms and expands, raising the temperature in the layer to 0°C and saturating the pore space to at least residual saturation levels (Colbeck, 1974). Consequently, where such conditions are present, the firn maintains a wet layer containing a quantifiable volume of liquid water – hereafter, referred to as the 1D Liquid Water Amount, LWA, with units of mm. The base of this wet layer is a freezing front due to the considerable cold content of the underlying firn, where winter's cold wave persists (Saito et al., 2024). As meltwater input diminishes or ceases in the autumn, the wet layer begins to freeze, both from the bottom upward and from the top downward.

This paper contrasts time series records of LWA from three sites in the percolation zone using records derived from four distinct methods. Two records are model based, representing meltwater and firn processes with varying complexity. One model is a polar regional climate model offering broad temporal and spatial coverage, while another utilizes higher fidelity physics initialized with site-specific conditions. The other two records were generated from analysis of physical measurements generated by in situ instrumentation and from a satellite platform. The latter relies on emerging methods for retrieval of L-band (1.4 GHz) radiometry signals and holds significant potential to become an important new tool for widespread ice sheet measurement. Our overarching objective is to evaluate the LWA time series generated from L-band radiometry, assessing both the performance of the method and the scientific merits of its data records. Each of the four LWA time series is imperfect due to limitations in the methodology. Consequently, a byproduct of our comparative analysis is an elucidation of the relative design limitations and performance shortcomings of each approach for determining liquid water in Greenland's percolation zone.

2. Methods

2.1. Sites and Years

We investigate three sites along the EGIG transect in western Greenland, approximately 100 km northeast of Jakobshaben Glacier (Figure 1). The sites are in the percolation zone and span a lateral distance of 30 km with elevations ranging from 1768 m to 2109 m. A strong gradient in the magnitude of summer meltwater generation exists between the sites, with Modèle Atmosphérique Régional (MAR) showing the 2010-2020 period averaged 373, 324, and 209 mm of melt at the study sites T3, T4, and UP18, respectively. As a result, the firn density and ice fraction (Harper et al., 2012) and firn temperatures (Saito et al., 2024) also show strong gradients between the sites.

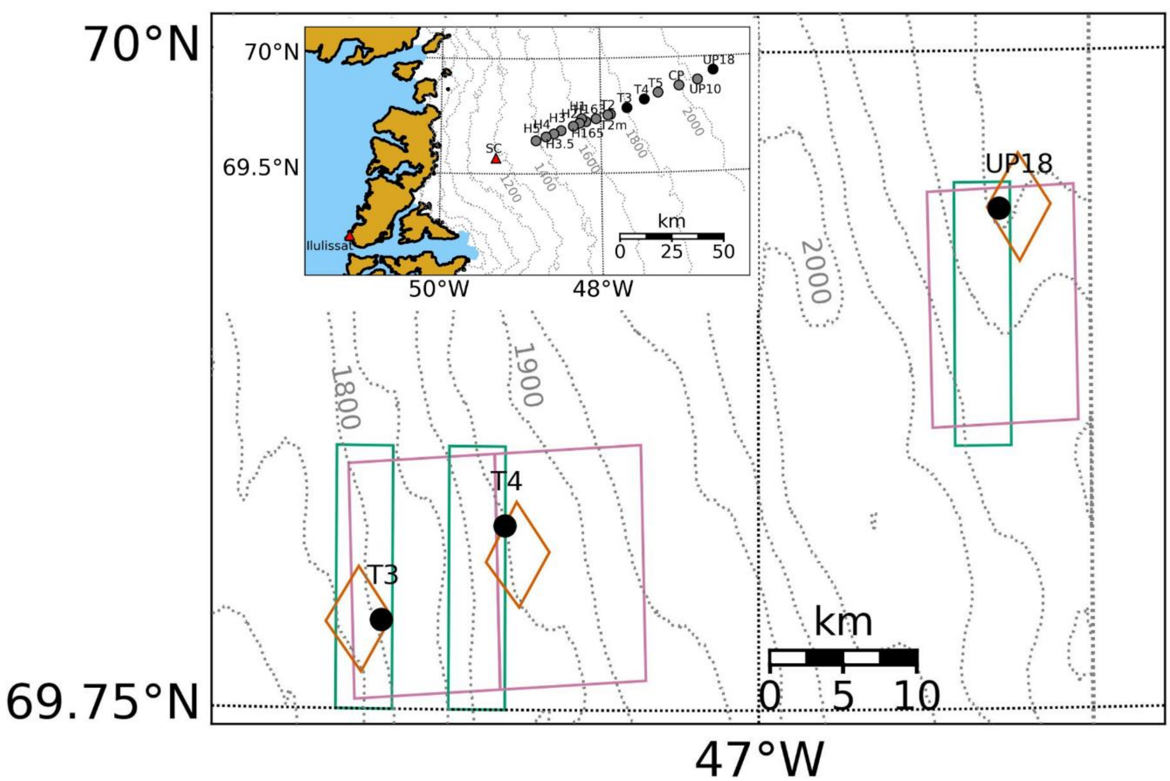

Figure 1. Map of the *in situ* data collection sites relative to Ilulissat, Greenland with elevation contours in grey dashed lines. Sites featured in this study as black dots, and relevant cells for MAR, L-Band retrieval, and ERA5 Land as purple, orange, and green boxes, respectively.

Our analysis compares the four methods of generating LWA at sites T4 and UP18, with time series extending over the summer of 2023, an exceptionally strong year (Ding et al., 2024; Poinar et al., 2023). As contrast, we also compare time series at site T3 during the relatively low melt summer of 2022 (Moon et al., 2022).

2.2. In Situ Observations

A time series of LWA in the firn column was calculated from in situ temperature time series. The temperature measurements were collected with strings of sensors installed in firn boreholes, which were then backfilled with snow. Sensors were digital temperature chips accurate to 0.1 ℃ with a resolution of 0.0078 ℃ and were spaced along the string at either 0.25 m or 0.33 m. Sensors were calibrated in the laboratory and potted in epoxy for water proofing and durability. Due to the electrically and thermally isolated environment in firn, the sensors show almost no noise at their maximum resolution. All sensor readings were recorded by a data logger installed on a pole at the surface. UP18 was installed in May 2023, whereas T4 and T3 were installed in May 2022. The 2023 time series at T4 was depth-adjusted to account for winter snow accumulation after installation.

Corresponding firn cores were also collected at each study site. The cores were logged for density and ice content in the field. The mass of core sections used in density calculations was measured using a calibrated electronic balance with 1g resolution, and ice content was determined by visual inspection.

To estimate the water content in the firn we first calculate the pore space capable of holding water based on the measured density profiles as:

$$\phi(z) = 1 - \frac{\rho(z)}{\rho_{close}}, \tag{1}$$

where $\rho(z)$ is the measured density at a given depth and ρ_{close} is the pore close off density in firn of 830 kg/m^3. Porosity curve and ice fraction are shown below in Figure 2.

Next, we extract the extent of the surface layer containing liquid water from the temperature time series. The minimum depth, z_{top}, and maximum depth, z_{bot}, of the 0° C isotherm define the extent of the wet layer across the time series (Figure 2). Assuming the wet layer is saturated to the residual saturation, 7% of the pore space in the firn (Colbeck, 1974), yields LWA as:

$$\mathrm{LWA} = \int_{z_{top}}^{z_{bot}} \phi(z)\ S_w\, dz\,, \tag{2}$$

where $\phi(z)$ is the porosity, S_w is the residual saturation and dz is the thickness of a given firn layer. So that diurnal fluctuations did not dominate seasonal signals, a smoothed time series of the 24 hour rolling mean of z_{top} was integrated using trapezoidal integration.

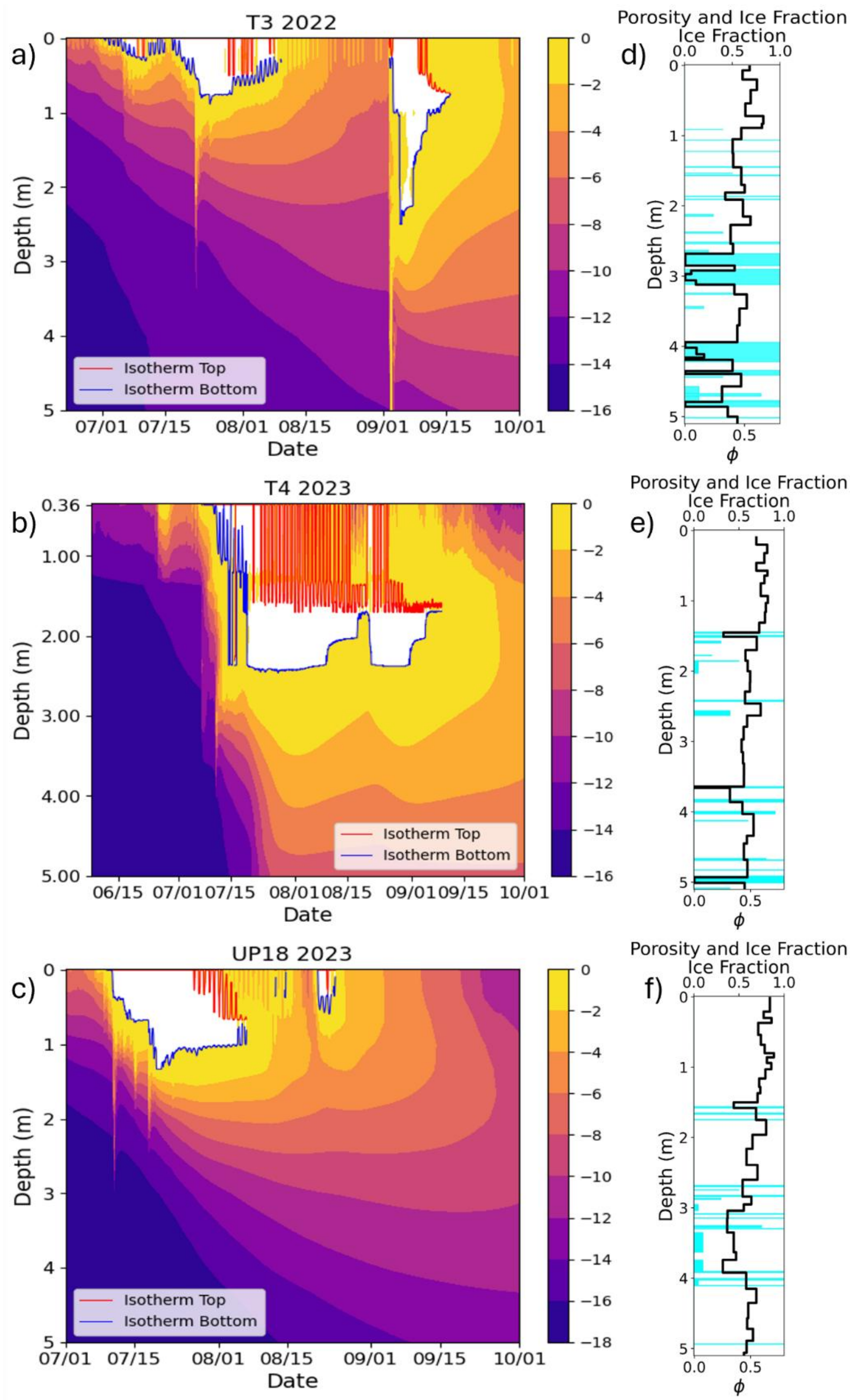

Figure 2. In situ measurements: a-c) temperature profiles in the upper 5 m of firn with the 0° C isotherm highlighted in white and its lower and upper bounds in red and blue, respectively; d-f) firn core measurements of ice fraction (cyan bars) and density-derived porosity (black line).

2.3. Remotely Sensed Observations

The LWA was retrieved from the L-band passive microwave brightness temperature (TB) measurements from the National Aeronautics and Space Administration (NASA) Soil Moisture Active Passive (SMAP) mission (Entekhabi et al. 2010). SMAP measures vertical and horizontal polarized TB with native 38-km resolution sampled from a 6 AM/PM equatorial crossing sun-synchronous orbit (Entekhabi et al., 2014; Piepmeier et al., 2017). The conically scanning, 40° incidence angle TB measurement results in a 1000-km swath width, allowing the measurement of the entire Greenland ice sheet twice daily. The enhanced-resolution TB products generated using the radiometer form of the Scatterometer Image Reconstruction (rSIR) algorithm and projected on the EASE-2 3.125 km grid (Long et al., 2019; Brodzik et al., 2019).

LWA was determined twice daily by matching the observed TB to TB simulated with a multilayer firn radiative transfer model (Mousavi et al., 2021). A wintertime TB signal was used to establish baseline absorptive and scattering properties unique to each site assuming no liquid water was present. A second post-melt season baseline signal was collected so that summer changes in the baseline conditions could be adjusted by linear interpolation between the two signals. The matching was done using look-up tables that were generated by sweeping over layer properties and parameters, such that the best fit between the simulated TB with differing water contents and the observed TB provides the estimate of LWA. The retrieved time series were linearly interpolated to 3-hour intervals for comparisons to modeled time series.

While L-band measurements provide a physical measurement, the method does not directly measure LWA. It relies on empirical models between the electrical properties of snow, firn, and ice and their physical properties (including LWA) (e.g., Hallikainen et al. 1986; Mousavi et al., 2022). In dry conditions, L-band signals can penetrate 100’s of meters through ice (Colliander et al., 2022; Rignot et al., 2001) but the presence of liquid water heavily attenuates signals so high LWA in the upper firn layers may block signals from deeper layers in the ice. However, for the typical summer liquid water contents in the percolation zone, L-band signals can penetrate through the surface wet layer, giving a total estimate of LWA (Colliander et al., 2022). This estimate represents the total instantaneous

LWA present in the firn column but as a result of assuming an average wet layer thickness does not resolve the depth-distributed liquid water profile (Hossan et al. 2024).

2.4. SLF-SNOWPACK model

The generation and storage of liquid water in the firn column was simulated using the physics-based snow and firn model, SLF-SNOWPACK (Bartelt & Lehning, 2002; Lehning et al., 2002), with forcing from ERA-5 climate reanalysis data (Muñoz-Sabater et al., 2021). We use SLF-SNOWPACK in its polar operational mode (Steger et al., 2017) with Richards flow infiltration (Wever et al., 2014, 2015) and Mo Hastings atmospheric handling (Holtslag & DeBruin, 1988). Simulations were initialized using the measured density and temperature profiles from each site and were run from April 1 through November 1 with 5-minute time steps. Based on field observations, this period begins prior to water input onset and ends after firn profiles have completely refrozen.

2.5. MAR Regional Climate Model Output

A second model simulation of LWA was provided by the MAR polar regional climate model driven by ERA5 reanalysis at 10km resolution (Fettweis et al., 2017, 2020.). Model outputs were obtained from University of Liège (see data availability). MAR provides a second modeled time series of LWA, although based on simplified physics and simulated over relatively large 10 by 10 km^2 cells. MAR employs a 20 m firn domain using a tipping bucket method for water infiltration. The mass fraction of water is recorded for each layer, along with the layer's density. We integrate this water fraction using trapezoidal integration and convert to its mm water equivalent as:

$$LWA = \frac{1000}{\rho_w} \int \rho(z)\theta_w(z)dz, \quad (3)$$

where $\rho(z)$ is the density of the firn, $\theta_w(z)$ is the mass fraction of water in the layer, dz is the thickness of the firn layer, and $\frac{1000}{\rho_w}$ is the conversion factor to convert the value to its mm water equivalent.

RESULTS

3.1 LWC time series

Both T4 and UP18 showed extensive development of surface wet layers during the summer of 2023 (Figure 3). Unusually deep and prolonged wet layers were driven by the exceptionally heavy melt year. For comparison, during another heavy melt year in 2019, Saito et al. (2024) observed no significant wet layer at CP, about halfway between the sites.

Measures such as melt duration and liquid water content were consistently higher at T4 due to its lower elevation (Figure 3). In addition to the large seasonal peak of LWA in the firn, smaller LWA peaks occurred both early and late in the 2023 season.

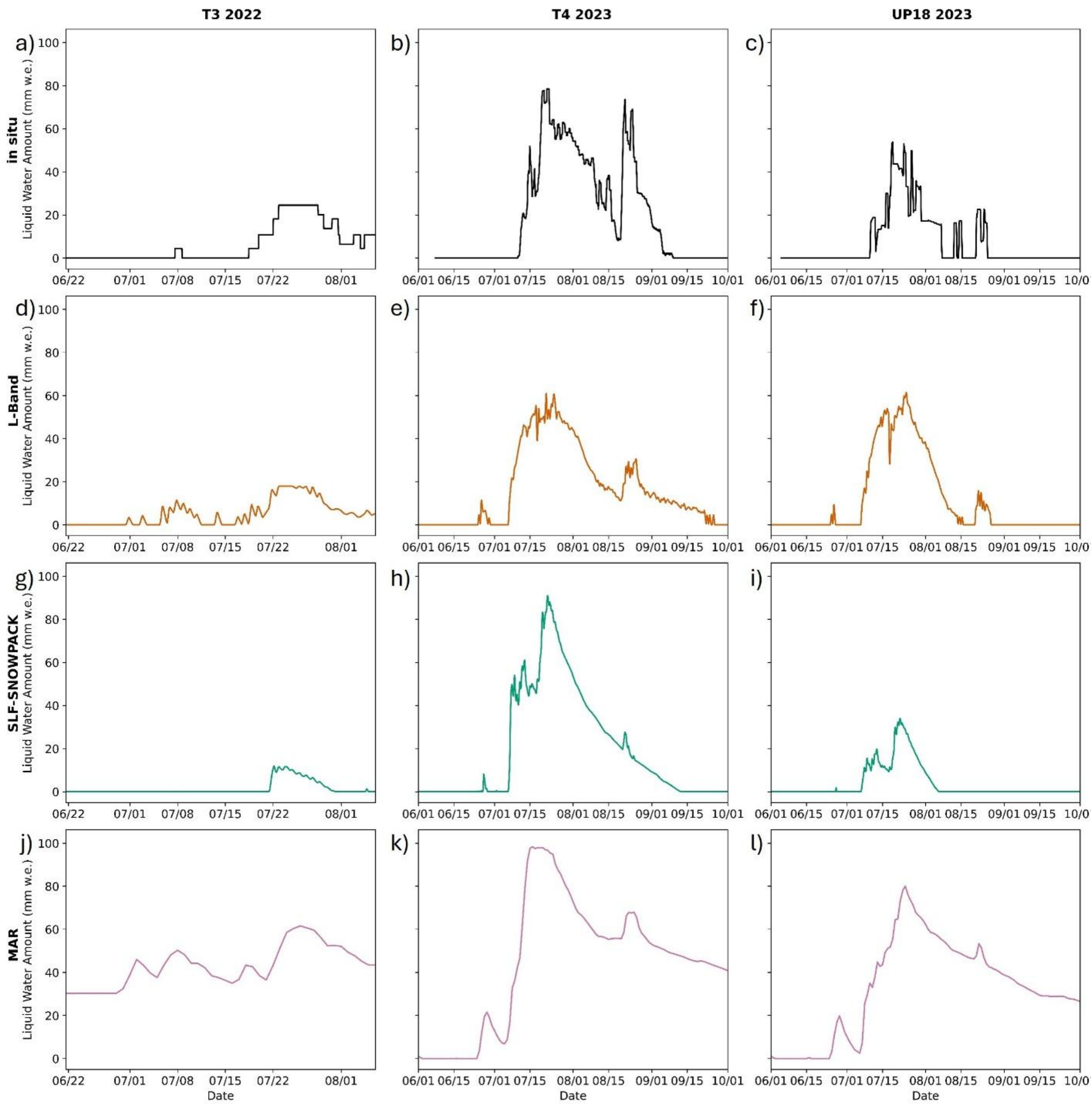

Figure 3. Time series of LWA for each site and record: a-c) in situ derived LWA (black); d-f) L-Band derived LWA (orange); g-i) SLF-SNOWPACK derived LWA (green); j-l) MAR derived LWA (purple). T3 2022 features a truncated date range due to a) the in situ record starting on June 6 and b) a SMAP outage from August 6 to October 16.

At T4, melt onset ranged from June 10 to July 24, depending on the data record. An early event of increasing LWA was observed in the SLF-SNOWPACK and L-band records, but not in the in situ record. Liquid water in the firn increased rapidly toward the seasonal peak, for example up to about 15 mm/day in the L-band record, before peaking and then refreezing at a slower rate. At peak around the third week of July, 58-98 mm of liquid water was in the firn column, depending on the record. MAR records consistently showed far more LWA than the other three records. Further, the MAR records retained liquid water until year-end, while the other three records showed liquid water present in the firn for around 2 months. The return to fully frozen conditions varied across these three records, from September 9 (in situ) to September 25 (L-band). The SFL-SNOWPACK record showed less sensitivity to late-season water influxes compared to other records.

Records from UP18 showed characteristics consistent with T4 but lower LWA in all but the L-band records. Liquid water onset occurred on June 24 in L-band records, followed by MAR one day later, and SLF-SNOWPACK and the in situ record delayed by 12 and 15 days, respectively. Maxima occurred in the four series within a 6-day window, when MAR showed 48% more LWA than the in situ records. Water persisted in the firn between 29 days (in situ) and 41 days (L-Band), with MAR again retaining liquid water through year-end. Fully frozen conditions returned August 6-26 in each record except MAR, which never refroze. The delayed onset and earlier refreeze in the in situ record was likely because there were no sensors near the surface leaving a shallow wet layer undetectable.

During the lower melt year of 2022, significantly less liquid water was present in the firn at T3 compared to the two higher elevation sites in 2023. Meltwater infiltration into the firn column occurred in early July across all methods except the SLF-SNOWPACK model and was followed by a refreezing episode. A second, larger increase in LWA was observed in late July and early August, but LWA maxima were minor compared to 2023. For instance, the peak L-band value at T3 in 2022 was less than one-third of the L-band maximum at T4 in 2023.

Overall, the MAR record exhibited the highest level of disagreement with other records, retaining liquid water from the previous year and consistently reporting greater LWA throughout the study period. For example, MAR's peak LWA at T4 in 2023 was 11%, 67%, and 30% higher than that reported by SLF-SNOWPACK, L-band, and in situ records, respectively. MAR also recorded rapid LWA fluctuations (>5 mm/day) in early July that were absent in SLF-SNOWPACK, while early-season melt detected by L-band was not captured by SLF-SNOWPACK and only minimally by in situ measurements. Across all methods, average nRMSE for LWA time series at each site ranged from 15% to 62%. The deviation between the two models, MAR and SLF-SNOWPACK, was far greater (nRMSE of 27%–133%) than between the two measurement-based methods, L-band and in situ (nRMSE of 9% to 17%). Thus, excluding MAR from the average nRMSE calculations resulted in higher agreement between measurement and model-based records, reducing nRMSE to 8%–13%.

Table 2. Statistical quantities concerning magnitude and variance of LWA curves.

Site	Record	Maximum LWA (mm)	Cumulative Refreezing Sum (mm)	RMSE* (mm)	nRMSE* (%)
T3 2022	in situ	25	33	4	17
	L-Band	18	86	-	-
	SLF-SNOWPACK	11	20	5	22
	MAR	62	50	38	210
T4 2023	in situ	75	292	9	15
	L-Band	59	209	-	-
	SLF-SNOWPACK	88	172	7	12
	MAR	98	87	29	49
UP18 2023	in situ	47	221	6	9
	L-Band	59	160	-	-
	SLF-SNOWPACK	32	66	8	13
	MAR	80	84	23	38

*calculated using L-Band timeseries as the reference value.

3.2 Cumulative Refreezing

The cumulative sum of negative changes in LWA represents net refreezing in the firn column (Figure 4). At site T4 in 2023, cumulative refreezing ranged from 87 to 292 mm w.e., where the in situ measurements showed the greatest values, followed by the L-Band, SLF-SNOWPACK, and MAR records. The SLF-SNOWPACK record showed all liquid water refrozen the earliest in autumn (Figure 3), while the MAR record never fully refroze all liquid water. Similarly, at UP18 in 2023, refreezing ranged from 65 to 220 mm w.e., in ascending order of SLF-SNOWPACK, MAR, L-Band, and in situ. Similarly, the SLF-SNOWPACK record showed no remaining LWA earliest. In contrast, during the low melt year at T3, the net refreezing was just 20–85 mm w.e., depending on the record. Further, the L-Band record showed the greatest value due to early water input events not captured in the other records.

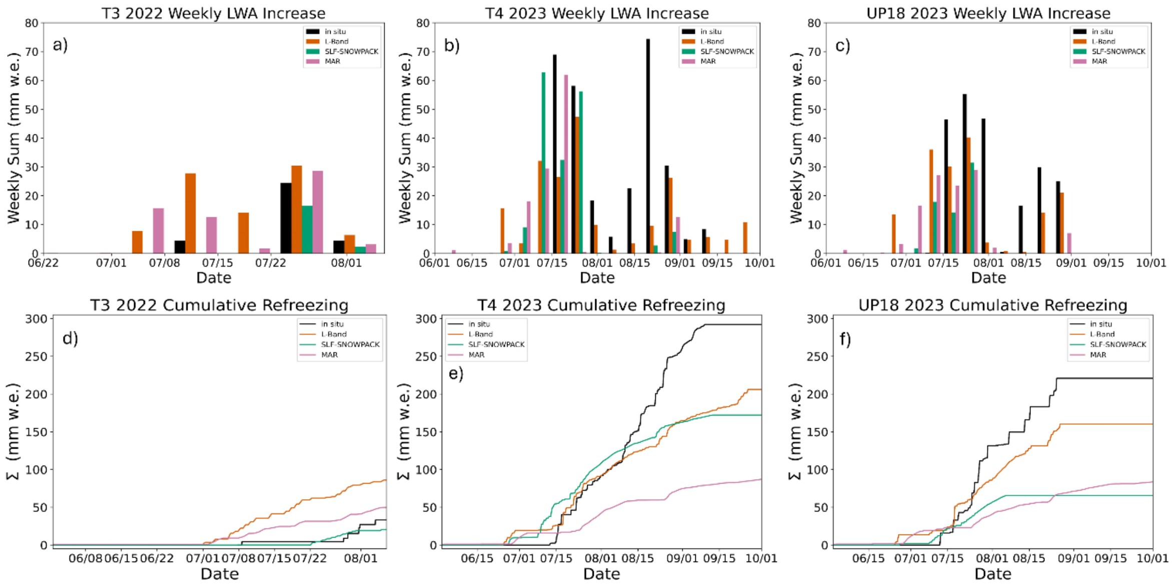

Figure 4. Water input and refreezing: a-c) liquid water entering firn calculated as the weekly sums of positive changes in the LWA timeseries; cumulative refreezing: d-f) calculated from the sum of decreases in the LWA time series.

4. Discussion

4.1 LWA Metric

Firn evolution in the percolation zone involves interactions of meltwater infiltration, refreezing, and firn compaction processes. These complexities necessitate reliable metrics to quantify changes in the firn's physical state, particularly for studies aiming to advance process level understanding or assess model performance. While temperature has been used as an assessment metric (Cox et al., 2015; Humphrey et al., 2012; Marchenko et al., 2021; Samimi et al., 2021), such records remain limited due to the logistical challenges of field installations. Other studies have relied on changes in density and ice content measured from consecutive firn cores to evaluate firn models (e.g.,Kuipers Munneke et al., 2015; Lundin et al., 2017). However, this approach faces several limitations: (a) density measurements typically average across ice layers and firn segments within each core section; (b) the discrete nature of firn coring prevents the generation of time-series data that could better capture processes and identify model performance issues; and (c) density changes between cores conflate compaction and meltwater processes, making it difficult to disentangle their individual effects.

The time series of LWA in the firn column offers a valuable alternative metric for quantifying the physical state of the firn. However, LWA records also have limitations as an assessment tool. LWA represents an instantaneous measurement of the cumulative effects of water input and refreezing. While changes in LWA are strongly correlated with these processes, the two signals are often intertwined, as water input and refreezing can occur simultaneously. Additionally, a single layer of firn may undergo multiple cycles of melt and refreezing. In such cases, the LWA metric may accurately reflect the heat balance but must be interpreted cautiously with respect to the overall mass balance of the firn.

4.2 Performance Shortcomings

Both observation-based and model-based methods for determining LWA time series have inherent design limitations (Table 1), resulting in varying characteristics of performance. No method achieves perfect fidelity to serve as a definitive standard for comparison. Our comparative analysis of LWA records, however, identifies several potential shortcomings of each approach.

Table 1. Selected benefits and limitations implicit to each method of LWA timeseries generation.

Method	Benefits	Limitations
In situ	- Observation based - High temporal resolution - No energy balance Parameterizations - Accounts for water lost to piping	- Assumed residual saturation - Discrete sensor positions - No near surface measurement - 1D point measurement - Logistically difficult to collect
L-Band	- Observation based - Ice sheet wide availability - Continuous data record - Sensitive to small fluxes	- Unresolved depth distribution - Twice daily measurements - Uncertain penetration depth in presence of high LWA - Signal processing impacted by refreezing and densification
SLF-SNOWPACK	- Solves Richards Equation - Initialized with measurements - Tracks many firn properties	- Piping not explicitly addressed - Uncertain parameterizations (e.g., clouds, albedo)
MAR	- Ice sheet scale - Includes SMB components	- Simple infiltration physics - Not initialized to measured firn column

• The MAR model propagated a wet layer far deeper into the firn than supported by in situ measurements or the SLF-SNOWPACK model. The winter cold wave failed to penetrate from the surface to such depths, and the model's lower boundary condition failed to simulate bottom-up refreezing, resulting in persistent liquid water in the firn column. However, this result is strongly contradicted by measurements of subfreezing firn temperature (e.g., -18° C) at multiple sites in the region (Saito et al., 2024) and is not observed in L-band or SLF-SNOWPACK records.

• The SLF-SNOWPACK model showed reduced sensitivity to small water input events compared to other methods. The model includes multiple parameters to refine meltwater generation, such as adjustments for cloud cover characteristics and surface albedo. However, robust observational targets would be necessary to confidently tune these parameters and improve accuracy.

• The in situ records are influenced by repeated melting and refreezing of firn layers at both the upper and lower boundaries of the wet layer. Diurnal freeze-thaw cycles during high melt periods caused particularly elevated totals and needed to be filtered out. Sensor spacing also caused stepwise changes in LWA and limited the sampling of shallow wet layers near the surface, reducing precision. Finally, the computed LWA was scaled by the assumed saturation level in the wet layer, which was set at a fixed value. Whereas S_w typically diminishes as snow sits at the melting point due to grain grounding and growth, saturation can also occasionally rise above S_w, particularly during episodes of high intensity water input.

• The L-band record has potential for measurement drift due to the design of the retrieval algorithm, relying on deviations in LWA induced summer TB from a baseline TB measurement. This baseline microwave emission reflects the internal density structure of the firn column under fully frozen conditions. During the summer melt season, the retrieval algorithm uses linear interpolation between consecutive winters to account for the evolving density structure. However, our records reveal the importance of episodic mid-season refreezing events, which deviate from a linear progression. As a result, the baseline TB should be lower, leading to an underestimation of liquid water at a given TB. Indeed, we see an amplified mismatch between the in situ records and L-band retrievals during the August 2023 increase of LWA. The discrepancy followed extensive refreezing since the seasonal peak a month earlier, likely altering the ice/density structure and the baseline emission signal.

Conclusions

We quantified the seasonal evolution of LWA in the firn column in Greenland's percolation zone at two relatively low-melt locations during a heavy melt year, and one higher-melt location during a low melt year. We find that LWA is a valuable metric for assessing the physical state of the firn, with time series of LWA offering insight into meltwater processes and serving as a measure of model performance. Observations and models show that LWA increases as a wet layer at the melting point expands downward, fed by water input at the surface. Refreezing of the wet layer occurs at the upper boundary due to a negative surface energy balance and at the lower boundary due to downward heat flux to cold firn at depth. LWA evolution in the firn column reflects the interplay between water input and refreezing processes, with changes occurring diurnally, episodically, and seasonally. Time series must be interpreted critically, as water influxes and refreezing often occur simultaneously, and individual firn layers may undergo multiple cycles of these events.

A comparison of four methods for determining LWA time series—two observational approaches (L-band radiometry and in situ temperature measurements) and two modeling approaches (MAR and SLF-SNOWPACK)—revealed notable agreement. Across all methods, normalized root mean square error (nRMSE) ranged from 15% to 62%, with the largest discrepancies observed between the MAR and SLF-SNOWPACK models (nRMSE 27% –132%, RMSE 27– 42 mm). Agreement between the observationally-based methods was significantly closer (nRMSE 9% – 17%, RMSE 3 – 8 mm). As none of the methods for generating LWA time series offer perfect fidelity due to design limitations, the comparisons identify the performance strengths and weaknesses of each method. The relative agreement of L-band radiometry with other methods for determining LWA in the firn column, particularly with in situ measurements and SLF-SNOWPACK, provides confidence in this emerging satellite-based observational technique. Radiometrically derived LWA time series thus show promise for generating insight into firn meltwater processes, and as a tuning target for improving model simulations of water infiltration and refreezing processes in the firn.

Data Availability

In situ Temperature and density data are publicly available from the arctic data center at doi:10.18739/A2DB7VR82, doi:10.18739/A2DB7VS0N, doi:10.18739/A28K74Z5S. MAR v3.14 10km daily forced by ERA5 is publicly available from University of Liège at http://phypc15.geo.ulg.ac.be/fettweis/MARv3.14/Greenland/ERA5-10km-daily/.
SMAP Radiometer Twice-Daily rSIR-Enhanced EASE-Grid 2.0 Brightness Temperatures, Version 2 data products 528 were provided by National Snow and Ice Data Center and are publicly available at https://nsidc.org/data/nsidc-0738/versions/2. ERA5 land used in forcing of SLF-SNOWPACK in available from the Copernicus Climate Data Store at https://cds.climate.copernicus.eu/datasets/reanalysis-era5-land?tab=overview. SLF-

SNOWPACK is provided by SLF under the LPGL version 3 open-source license and is available at https://code.wsl.ch/snow-models/snowpack/-/releases.

Acknowledgements

Funded by grants from NSF (#2119689 and #2113391). A contribution to this work was made at the Jet Propulsion Laboratory, California Institute of Technology, under a contract with the National Aeronautics and Space Administration.

References

Amory, C., Buizert, C., Buzzard, S., Case, E., Clerx, N., Culberg, R., Datta, R. T., Dey, R., Drews, R., Dunmire, D., Eayrs, C., Hansen, N., Humbert, A., Kaitheri, A., Keegan, K., Kuipers Munneke, P., Lenaerts, J. T. M., Lhermitte, S., Mair, D., ... Wouters, B. (2024). Firn on ice sheets. In *Nature Reviews Earth and Environment* (Vol. 5, Issue 2, pp. 79–99). Springer Nature. https://doi.org/10.1038/s43017-023-00507-9

Bartelt, P., & Lehning, M. (2002). *A physical SNOWPACK model for the Swiss avalanche warning Part I: numerical model*. www.elsevier.com/locate/coldregions

Benson, C. S. (1962). *Stratigraphic Studies in the Snow and Firn of the Greenland Ice Sheet*.

Braithwaite, R. J., Laternser, M., & Pfeffer, W. T. (1994). Variations of near-surface firn density in the lower accumulation area of the Greenland ice sheet, Pâkitsoq, West Greenland. *Journal of Glaciology*, *40*(136), 477–485. https://doi.org/10.3189/s002214300001234x

Brodzik, M. J., Long, D. G. & Hardman, M. A. (2019). SMAP Radiometer Twice-Daily rSIR-Enhanced EASE-Grid 2.0 Brightness Temperatures. (NSIDC-0738, Version 1). Boulder, Colorado USA. NASA National Snow and Ice Data Center Distributed Active Archive Center. https://doi.org/10.5067/QZ3WJNOUZLFK.

Colbeck, S. C. (1974). The capillary effects on water percolation in homogeneous snow. *Journal of Glaciology*, *13*(67), 85–97. https://doi.org/10.3189/s002214300002339x

Colliander, A., Mousavi, M., Marshall, S., Samimi, S., Kimball, J. S., Miller, J. Z., Johnson, J., & Burgin, M. (2022). Ice Sheet Surface and Subsurface Melt Water Discrimination Using Multi-Frequency Microwave Radiometry. *Geophysical Research Letters*, *49*(4). https://doi.org/10.1029/2021GL096599

Cox, C., Humphrey, N., & Harper, J. (2015). Quantifying meltwater refreezing along a transect of sites on the Greenland ice sheet. *Cryosphere*, *9*(2), 691–701. https://doi.org/10.5194/tc-9-691-2015

Culberg, R., Schroeder, D. M., & Chu, W. (2021). Extreme melt season ice layers reduce firn permeability across Greenland. *Nature Communications*, *12*(1). https://doi.org/10.1038/s41467-021-22656-5

Ding, M. H., Wang, X., Bian, L. G., Jiang, Z. N., Lin, X., Qu, Z. F., Su, J., Wang, S., Wei, T., Zhai, X. C., Zhang, D. Q., Zhang, L., Zhang, W. Q., Zhao, S. D., & Zhu, K. J. (2024). State of polar climate in 2023. *Advances in Climate Change Research*, *15*(5), 769–783. https://doi.org/10.1016/J.ACCRE.2024.08.004

Entekhabi, D., Njoku, E. G., O'Neill, P. E., Kellogg, K. H., Crow, W. T., Edelstein, W. N., Entin, J. K., Goodman, S. D., Jackson, T. J., Johnson, J., Kimball, J., Piepmeier, J. R., Koster, R. D., Martin, N., McDonald, K. C., Moghaddam, M., Moran, S., Reichle, R., Shi, J. C., Spencer, M. W., Thurman, S. W., Tsang, L., and Van Zyl, J.: The soil moisture active passive (SMAP) mission, Proc. IEEE, 98, 704–716, https://doi.org/10.1109/JPROC.2010.2043918, 2010.

Entekhabi, D., S. Yueh, P. O'Neill, and K. Kellogg. (2014). SMAP Handbook – Soil Moisture Active Passive: Mapping Soil Moisture and Freeze/Thaw from Space. SMAP Project, Jet Propulsion Laboratory, Pasadena, CA.

Fettweis, X., Box, J. E., Agosta, C., Amory, C., Kittel, C., Lang, C., Van As, D., Machguth, H., & Gallée, H. (2017). Reconstructions of the 1900-2015 Greenland ice sheet surface mass balance using the regional climate MAR model. *Cryosphere*, *11*(2), 1015–1033. https://doi.org/10.5194/tc-11-1015-2017

Fettweis, X., Hofer, S., Krebs-Kanzow, U., Amory, C., Aoki, T., Berends, C. J., Born, A., Box, J. E., Delhasse, A., Fujita, K., Gierz, P., Goelzer, H., Hanna, E., Hashimoto, A., Huybrechts, P., Kapsch, M. L., King, M. D., Kittel, C., Lang, C., … Zolles, T. (2020). GrSMBMIP: Intercomparison of the modelled 1980-2012 surface mass balance over the Greenland Ice Sheet. *Cryosphere*, *14*(11), 3935–3958. https://doi.org/10.5194/tc-14-3935-2020

Forster, R. R., Box, J. E., Van Den Broeke, M. R., Miège, C., Burgess, E. W., Van Angelen, J. H., Lenaerts, J. T. M., Koenig, L. S., Paden, J., Lewis, C., Gogineni, S. P., Leuschen, C., & McConnell, J. R. (2014). Extensive liquid meltwater storage in firn within the Greenland ice sheet. *Nature Geoscience*, *7*(2), 95–98. https://doi.org/10.1038/ngeo2043

Hallikainen, M., Ulaby, F., & Abdelrazik, M. (1986). Dielectric properties of snow in the 3 to 37 GHz range. In IEEE Transactions on Antennas and Propagation (Vol. 34, Issue 11, pp. 1329–1340). Institute of Electrical and Electronics Engineers (IEEE). https://doi.org/10.1109/tap.1986.1143757 34(11), 1329–1340.

Harper, J., Humphrey, N., Pfeffer, W. T., Brown, J., & Fettweis, X. (2012). Greenland ice-sheet contribution to sea-level rise buffered by meltwater storage in firn. *Nature*, *491*(7423), 240–243. https://doi.org/10.1038/nature11566

Holtslag, A. A. M., & DeBruin. (1988). Mo_holtsagAtmosphericHoltslag1988JAMC. *Journal of Applied Meteorology and Climatology*. https://doi.org/https://doi.org/10.1175/1520-0450(1988)027<0689:AMOTNS>2.0.CO;2

Hossan, A., Colliander, A., Vandecrux, B., Schlegel, N.-J., Harper, J., Marshall, S., and Miller, J. Z.: Retrieval and Validation of Total Seasonal Liquid Water Amounts in the Percolation Zone of Greenland Ice Sheet Using L-band Radiometry, EGUsphere [preprint], https://doi.org/10.5194/egusphere-2024-2563, 2024.

Houtz, D., Mätzler, C., Naderpour, R., Schwank, M., and Steffen, K.: Quantifying Surface Melt and Liquid Water on the Greenland Ice Sheet using L-band Radiometry, Remote Sens. Environ., https://doi.org/10.1016/j.rse.2021.112341, 2021.

Humphrey, N. F., Harper, J. T., & Pfeffer, W. T. (2012). Thermal tracking of meltwater retention in Greenland's accumulation area. *Journal of Geophysical Research: Earth Surface*, *117*(1). https://doi.org/10.1029/2011JF002083

Kerr, Y. H., Waldteufel, P., Wigneron, J.-P., Delwart, S., Cabot, F., Boutin, J., Escorihuela, M.-J., Font, J., Reul, N., Gruhier, C., Juglea, S. E., Drinkwater, M. R., Hahne, A., Martín-Neira, M., & Mecklenburg, S. (2010). The SMOS Mission: New Tool for Monitoring Key Elements of the Global Water Cycle. Proceedings of the IEEE (Vol. 98, Issue 5, pp. 666–687). https://doi.org/10.1109/jproc.2010.2043032

Kuipers Munneke, P., Ligtenberg, S. R. M., Noël, B. P. Y., Howat, I. M., Box, J. E., Mosley-Thompson, E., McConnell, J. R., Steffen, K., Harper, J. T., Das, S. B., & van den Broeke, M. R. (2015). Elevation change of the Greenland Ice Sheet due to surface mass balance and firn processes, 1960–2014. *The Cryosphere*, *9*(6), 2009–2025. https://doi.org/10.5194/tc-9-2009-2015

Lehning, M., Bartelt, P., Brown, B., Fierz, C., & Satyawali, P. (2002). *A physical SNOWPACK model for the Swiss avalanche warning Part II. Snow microstructure*. www.elsevier.com/locate/coldregions

Long, D. G., Brodzik, M. J., and Hardman, M. A.: Enhanced-resolution SMAP brightness temperature image products, IEEE Trans. Geosci. Remote Sens., 57(7), 4151–4163, doi:10.1109/TGRS.2018.2889427, 2019.

LUNDIN, J. M. D., STEVENS, C. M., ARTHERN, R., BUIZERT, C., ORSI, A., LIGTENBERG, S. R. M., SIMONSEN, S. B., CUMMINGS, E., ESSERY, R., LEAHY, W., HARRIS, P., HELSEN, M.

M., & WADDINGTON, E. D. (2017). Firn Model Intercomparison Experiment (FirnMICE). *Journal of Glaciology*, *63*(239), 401–422. https://doi.org/10.1017/jog.2016.114

Machguth, H., Macferrin, M., Van As, D., Box, J. E., Charalampidis, C., Colgan, W., Fausto, R. S., Meijer, H. A. J., Mosley-Thompson, E., & Van De Wal, R. S. W. (2016). Greenland meltwater storage in firn limited by near-surface ice formation. *Nature Climate Change*, *6*(4), 390–393. https://doi.org/10.1038/nclimate2899

Marchenko, S. A., Van Pelt, W. J. J., Pettersson, R., Pohjola, V. A., & Reijmer, C. H. (2021). Water content of firn at Lomonosovfonna, Svalbard, derived from subsurface temperature measurements. *Journal of Glaciology*, *67*(265), 921–932. https://doi.org/10.1017/jog.2021.43

Marsh, P., & Woo, M. -K. (1984). Wetting front advance and freezing of meltwater within a snow cover: 1. Observations in the Canadian Arctic. *Water Resources Research*, *20*(12), 1853–1864. https://doi.org/10.1029/WR020i012p01853

Miller, J. Z., Culberg, R., Long, D. G., Shuman, C. A., Schroeder, D. M., & Brodzik, M. J. (2022). An empirical algorithm to map perennial firn aquifers and ice slabs within the Greenland Ice Sheet using satellite L-band microwave radiometry. *The Cryosphere*, *16*(1), 103–125. https://doi.org/10.5194/tc-16-103-2022

Moon, T. A., Mankoff, K. D., Fausto, R. S., Fettweis, X., Loomis, B. D., Mote, T. L., Poinar, K., Tedesco, M., Wehrlé, A., & Jensen, C. D. (2022). Greenland Ice Sheet. *NOAA Technical Report OAR ARC*. https://doi.org/10.25923/c430-hb50

Mousavi, M., Colliander, A., Miller, J. Z., Entekhabi, D., Johnson, J. T., Shuman, C. A., Kimball, J. S., & Courville, Z. R. (2021). Evaluation of Surface Melt on the Greenland Ice Sheet Using SMAP L-Band Microwave Radiometry. *IEEE Journal of Selected Topics in Applied Earth Observations and Remote Sensing*, *14*, 11439–11449. https://doi.org/10.1109/JSTARS.2021.3124229

Mousavi, S., A. Colliander, J.Z. Miller, J.S. Kimball. (2022). A Novel Approach to Map the Intensity of Surface Melting on the Antarctica Ice Sheet using SMAP L-Band Microwave Radiometry, IEEE J. Sel. Topics Appl. Earth Obs. Remote Sens. vol. 15, pp. 1724-1743, 2022, doi: 10.1109/JSTARS.2022.3147430

Muñoz-Sabater, J., Dutra, E., Agustí-Panareda, A., Albergel, C., Arduini, G., Balsamo, G., Boussetta, S., Choulga, M., Harrigan, S., Hersbach, H., Martens, B., Miralles, D. G., Piles, M., Rodríguez-Fernández, N. J., Zsoter, E., Buontempo, C., & Thépaut, J. N. (2021). ERA5-Land: A state-of-the-art global reanalysis dataset for land applications.

Earth System Science Data, *13*(9), 4349–4383. https://doi.org/10.5194/essd-13-4349-2021

Parry, V., Nienow, P., Mair, D., Scott, J., Hubbard, B., Steffen, K., & Wingham, D. (2007). Investigations of meltwater refreezing and density variations in the snowpack and firn within the percolation zone of the Greenland ice sheet. *Annals of Glaciology*, *46*, 61–68. https://doi.org/10.3189/172756407782871332

Piepmeier, J. R., Focardi, P., Horgan, K. A., Knuble, J., Ehsan, N., Lucey, J., Brambora, C., Brown, P. R., Hoffman, P. J., French, R. T., Mikhaylov, R. L., Kwack, E.-Y., Slimko, E. M., Dawson, D. E., Hudson, D., Peng, J., Mohammed, P. N., De Amici, G., Freedman, A. P., ... Njoku, E. G. (2017). SMAP L-Band Microwave Radiometer: Instrument Design and First Year on Orbit. IEEE Transactions on Geoscience and Remote Sensing, 55(4), 1954–1966. https://doi.org/10.1109/tgrs.2016.2631978

Poinar, K., Mankoff, K. D., Fausto, R. S., Fettweis, X., Loomis, B. D., Wehrlé, A., Jensen, C. D., Tedesco, M., Box, J. E., & Mote, T. L. (2023). NOAA Arctic Report Card: Greenland Ice Sheet. *NOAA Technical Report OAR ARC*. https://doi.org/10.25923/yetx-rs76

Reijmer, C. H., van den Broeke, M. R., Fettweis, X., Ettema, J., & Stap, L. B. (2012). Refreezing on the Greenland ice sheet: a comparison of parameterizations. *The Cryosphere*, *6*(4), 743–762. https://doi.org/10.5194/tc-6-743-2012

Rignot, E., Echelmeyer, K., & Krabill, W. (2001). Penetration depth of interferometric synthetic-aperture radar signals in snow and ice. *Geophysical Research Letters*, *28*(18), 3501–3504. https://doi.org/10.1029/2000GL012484

Saito, J., Harper, J., & Humphrey, N. (2024). Uptake and Transfer of Heat Within the Firn Layer of Greenland Ice Sheet's Percolation Zone. *Journal of Geophysical Research: Earth Surface*, *129*(6). https://doi.org/10.1029/2024JF007667

Samimi, S., Marshall, S. J., & MacFerrin, M. (2020). Meltwater Penetration Through Temperate Ice Layers in the Percolation Zone at DYE-2, Greenland Ice Sheet. *Geophysical Research Letters*, *47*(15). https://doi.org/10.1029/2020GL089211

Samimi, S., Marshall, S. J., Vandecrux, B., & MacFerrin, M. (2021). Time-Domain Reflectometry Measurements and Modeling of Firn Meltwater Infiltration at DYE-2, Greenland. *Journal of Geophysical Research: Earth Surface*, *126*(10). https://doi.org/10.1029/2021JF006295

Steger, C. R., Reijmer, C. H., van den Broeke, M. R., Wever, N., Forster, R. R., Koenig, L. S., Munneke, P. K., Lehning, M., Lhermitte, S., Ligtenberg, S. R. M., Miège, C., & Noël, B. P.

Y. (2017). Firn meltwater retention on the greenland ice sheet: A model comparison. *Frontiers in Earth Science*, *5*. https://doi.org/10.3389/feart.2017.00003

Vandecrux, B., Mottram, R., Langen, P. L., Fausto, R. S., Olesen, M., Stevens, C. M., Verjans, V., Leeson, A., Ligtenberg, S., Kuipers Munneke, P., Marchenko, S., van Pelt, W., Meyer, C. R., Simonsen, S. B., Heilig, A., Samimi, S., Marshall, S., Machguth, H., MacFerrin, M., ... Box, J. E. (2020). The firn meltwater Retention Model Intercomparison Project (RetMIP): evaluation of nine firn models at four weather station sites on the Greenland ice sheet. *The Cryosphere*, *14*(11), 3785–3810. https://doi.org/10.5194/tc-14-3785-2020

Wever, N., Fierz, C., Mitterer, C., Hirashima, H., & Lehning, M. (2014). Solving Richards Equation for snow improves snowpack meltwater runoff estimations in detailed multi-layer snowpack model. *Cryosphere*, *8*(1), 257–274. https://doi.org/10.5194/tc-8-257-2014

Wever, N., Schmid, L., Heilig, A., Eisen, O., Fierz, C., & Lehning, M. (2015). Verification of the multi-layer SNOWPACK model with different water transport schemes. *Cryosphere*, *9*(6), 2271–2293. https://doi.org/10.5194/tc-9-2271-2015